lengths than would be accessible with the usual crystal monochromator (Section 2.3.4.1.2). The idea of supermirrors, comprising bilayers of graduated thickness, and in effect increasing the critical angle, was suggested by Turchin (1967) and Mezei (1976). For a perhaps simplistic explanation, we note first that since the bilayer dimension d is large compared with the neutron wavelength, we can approximate the above equation for reflection as

$$\theta \simeq \lambda \frac{1}{2d},$$

in which form it is reminiscent of equation (2.3.6). If we take $d_{\min}$ to be the thickness of the thinnest bilayer, then we can propose that the critical angle for reflection by the supermirror should be

$$\theta_c^{\rm SM} \simeq \lambda \frac{1}{2d_{\min}}. \qquad (2.3.13)$$

In order to ensure that all neutrons incident at angles less than this critical angle should be reflected, we need to incorporate a more-or-less continuous range of thicker bilayers into the supermirror (Fig. 2.3.14*b*). A more rigorous treatment (Hayter & Mook, 1989; Masalovich, 2013) takes account of the transmission and reflection at each interface, and lays down a prescription as to how the thicknesses should be varied. The most common pairing for the bilayer is now Ni with Ti; the coherent scattering cross sections are of opposite sign (see Table 2.3.2). The performance of a supermirror is normally quoted as the ratio m of the critical angle for the supermirror, $\theta_c^{\rm SM}$, to that for natural nickel, $\theta_c^{\rm Ni}$; a high value for reflectivity is also important. Supermirrors to m of 2 or 3 are in quite common use, while now Ni/Ti supermirrors with m up to 7 are offered for purchase (Swiss Neutronics AG; see also Maruyama *et al.*, 2007).

Consideration is currently being given to the variation of the cross section of the guide along its length. There is some loss on reflection by supermirrors, so these studies aim to reduce the number of reflections involved in transmission along the guide. One suggestion (also attributable to Mezei, 1997) is to use a 'ballistic guide', in which neutrons from the source travel through a taper of widening cross section into a length of larger guide, then through a taper of narrowing cross section to restore the original cross section at the exit. This is said to reduce the number of reflections suffered by the neutron by a factor of $(w_0/w)^2$, where w_0 is the width at entrance and exit and w the larger width along the main part of the guide (Häse *et al.*, 2002). Such a guide has been installed and is operating successfully on the vertical cold source at the Institut Laue–Langevin (Abele *et al.*, 2006). An extension of this idea is based on the well known property of ellipses that a ray emanating from one focus is reflected (just one bounce) to pass through the other; so if the guide cross section could be varied to give a very long ellipse, a source of neutrons placed at one focus, and the target point at the other, then perhaps the neutrons could be transmitted along the guide with just a single reflection (Schanzer *et al.*, 2004; Rodriguez *et al.*, 2011). Accordingly a number of neutron facilities have installed elliptical guides, and indeed a number of neutron powder diffractometers now are located on elliptical guides; these include diffractometer POWTEX at FRM-II, the high-resolution diffractometers HRPD and WISH at ISIS, and Super-HRPD at JSNS. Computer simulation by Cussen *et al.* (2013), however, questions whether, given the practicalities of finite source sizes and the approximation of elliptical variation by a number of linear segments, the theoretical improvement is fully realized.

2.3.4. Diffractometers

Put simply, the diffracted neutron beams associated with the different d-spacings in the sample under study satisfy Bragg's law,

$$\lambda = 2d \sin(\theta). \qquad (2.3.14)$$

As always, λ is the wavelength of the incident neutrons, and these neutrons are scattered through an angle 2θ.

There are basically two ways of exploiting this relationship. The first is to use a single wavelength for the investigation, in which case diffracted neutrons are observed at different angles 2θ corresponding to different d-spacings in the sample. A neutron powder diffractometer designed to carry out an investigation by this means we choose to call a 'constant wavelength' (CW) diffractometer. The other means is to fix the angle 2θ, illuminate the specimen with a range of wavelengths, and note the different wavelengths that are diffracted. In this case, we determine the wavelengths of the diffracted neutrons *via* their speed $\lambda = h/(mv)$ [equation (2.3.1)], and that in turn is measured by their flight time t over a path of length L, $v = L/t$; this leads to

$$\lambda = \frac{ht}{mL}. \qquad (2.3.15)$$

A diffractometer designed to carry out such an analysis of wavelengths we call a 'time-of-flight (TOF) diffractometer'.

The distinction between these two modes of operation can also be indicated *via* the Ewald construction in reciprocal space (Section 1.1.2.4). In this, the ideal powder is represented by concentric spheres in reciprocal space. In the constant-wavelength situation, the primary beam is fixed in direction and the Ewald sphere has a fixed radius; diffracted (reflected) beams are observed at any angle at which the surface of the Ewald sphere intersects one of the concentric spheres mentioned just above. In the wavelength-analysis (time-of-flight) situation, the directions of the primary and diffracted beams are fixed, but the radius of the Ewald sphere ($1/\lambda$) is variable through a range; diffracted beams are observed whenever the wavelength is such that the tip of the vector representing the reflected beam lies on one of the concentric spheres.

2.3.4.1. *Constant-wavelength neutron diffractometers*

The salient features of a constant-wavelength diffractometer are perhaps most easily explained by reference to a particular example; for this purpose we consider the High Resolution Powder diffractometer for Thermal neutrons (HRPT) installed at the SINQ continuous spallation source (Fischer *et al.*, 2000). Neutrons from the source travel through a guide tube to the crystal monochromator, which directs neutrons of a selected wavelength toward the sample. The diffracted neutrons are registered in a detector or detectors that cover a range of angles of scattering from the sample. Collimation is used to better define the directions of the neutron beams; in this instance a primary collimator is included in the guide tube and additional collimation is included between the sample and the position-sensitive detector. The various components will be described in more detail below.

2.3.4.1.1. *Collimation*

There need to be restrictions on the angular divergences of the neutron beams. The divergence of the beam impinging upon the crystal monochromator must be limited to better define the wavelength of the neutrons directed to the sample, whereas the divergences of the beams incident upon and diffracted from

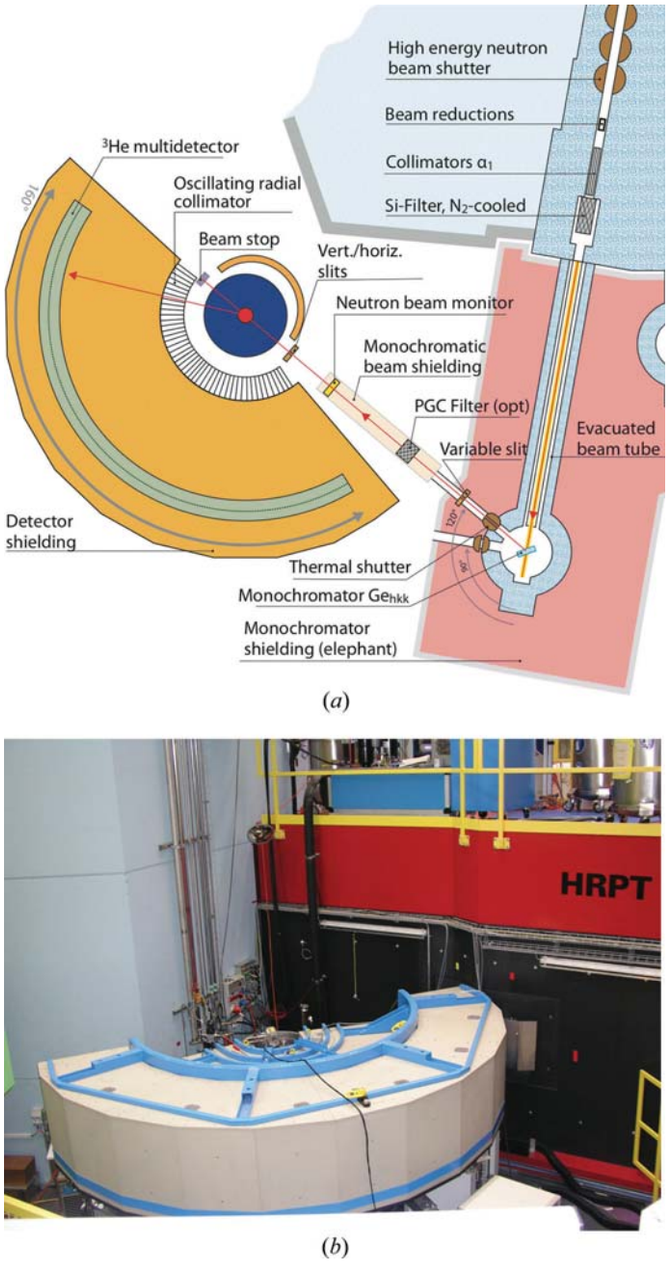

Figure 2.3.15
A constant-wavelength neutron powder diffractometer. This figure shows (*a*) a layout diagram and (*b*) the physical appearance (dominated by the monochromator and detector shieldings) for the HRPT diffractometer installed at the SINQ continuous spallation source. (Figures from https://www.psi.ch/sinq/hrpt/.)

the sample will control the precision with which the scattering angle 2θ can be determined. For a diffractometer detecting neutrons and measuring scattering angles in the horizontal plane (as shown in Fig. 2.3.15) the horizontal divergences are critical, the vertical divergences less so.[11] Indeed, the horizontal divergences are key parameters in the determination of resolution and intensity (Section 2.3.4.1.4); for this reason we denote by α_1, α_2 and α_3 the (half-angle) angular divergences of the primary beam (*i.e.* the beam onto the monochromator), the monochromatic beam (from monochromator to sample) and the diffracted beam (from sample to detector), respectively.

[11] For this reason large vertical divergences are employed to increase intensity; they do however have second-order impacts on the shapes (asymmetry) and positions of diffraction peaks (Howard, 1982; Finger *et al.*, 1994; see also Section 4.2 in Kisi & Howard, 2008).

The divergences are limited by various forms of collimation. The divergence of the primary beam will be limited in the first instance by the delivery system. For delivery through a simple beam tube of length L, with entrance and exit apertures of dimensions a_1 and a_2, respectively, the angular divergence (half-angle) is given by (as already noted in Section 2.3.3.4)

$$\alpha_1 = \frac{a_1 + a_2}{2L}. \tag{2.3.16}$$

Neutrons emerging from a guide tube would have divergence equal to the critical angle of the guide, $\alpha_1 = \theta_c$. Soller collimators (see below) can be used if there is a need to further reduce the horizontal divergence of the primary beam. The divergence of the monochromatic beam may be limited by slits, or a beam tube. The divergence of the diffracted beam, α_3, is often defined using another Soller collimator. Sometimes this divergence is limited just by the dimensions of the sample and the detecting elements; equation (2.3.16) gives α_3 if it now references the sample and detector element dimensions and the distance between them. Even in this circumstance (as in HRPT), Soller collimators may be used in front of the detector to reduce scattering from ancillary equipment and other background contributions.

Soller collimators (Soller, 1924) are used to transmit beams of large cross section while limiting (for example) horizontal divergence. They are in effect narrow but tall rectangular collimators stacked side by side; in practice they comprise thin neutron-absorbing blades equally spaced in a mounting box. It should be evident from equation (2.3.16) that if the length of the collimator is L and the separation between the blades is a, then the (half-angle) horizontal divergence is a/L. The transmission function for a Soller collimator is ideally triangular. It is technologically challenging to make compact Soller collimators, since, for a given collimation, a shorter collimator needs a smaller blade spacing. One very successful approach, due to Carlile *et al.* (1977), has been to make the neutron-absorbing blades from Mylar, stretched on thin steel or aluminium alloy frames, and subsequently coated with gadolinium oxide paint; these blades are stacked and connected *via* the frames which become the spacers in the final product. The collimators made by Carlile *et al.* were 34 cm long, and the blade spacing was 1 mm, giving a horizontal divergence of 0.17°. Compact Soller collimators of this type (Fig. 2.3.16) are now commercially available, with blade spacings down to 0.5 mm.

Even more compact collimators can be produced by eliminating the gaps in favour of solid layers of neutron-transmitting material; for example, a collimator only 2.75 cm long made by stacking 0.16 mm thick gadolinium-coated silicon wafers gave a divergence of 0.33° (Cussen *et al.*, 2001). Microchannel plates (Wilkins *et al.*, 1989) may offer additional possibilities for collimation and focusing.

2.3.4.1.2. *Monochromators*

The wavelength in a constant-wavelength powder diffractometer is almost invariably selected by a single-crystal monochromator. If the primary beam is incident onto the monochromator in such a way as to make an angle θ_M with a chosen set of planes in the crystal, then the wavelength that will be reflected from these planes is given by Bragg's law,

$$\lambda = 2d \sin(\theta_M),$$

where d is the spacing of the chosen planes. A spread of angles of incidence represented by $\Delta\theta_M$ will result in the selection of a

Figure 2.3.16
Commercially available compact Soller collimators. (Reproduced with permission from Eurocollimators Ltd, UK.)

band of wavelengths $\Delta\lambda$ given by

$$\frac{\Delta\lambda}{\lambda} = \cot\theta_M \Delta\theta_M. \qquad (2.3.17)$$

For high-resolution performance we need a rather precisely defined wavelength, so $\Delta\lambda$ should be small; if, on the other hand, intensity is an issue then a wider band of wavelengths needs to be accepted. It should be evident from equation (2.3.17) that a high-resolution diffractometer will operate with a take-off angle from the monochromator, $2\theta_M$, as high (*i.e.* as close to 180°) as practicable, and with tight primary collimation α_1.

It might be noticed that the integer n appearing on the right-hand side of equation (1.1.3) has been omitted from our formulation of Bragg's law. If the Miller indices of the chosen planes are hkl, if the spacing of these planes is d_{hkl}, and if we introduce $d_{nh,nk,nl} = d_{hkl}/n$ [*cf.* equation (1.1.23)], then the factor n is effectively restored. This means that, as well as reflecting the selected wavelength through the hkl reflection, the monochromator has the potential to reflect unwanted harmonics λ/n of the desired wavelength through the nh,nk,nl reflections. This problem can be largely overcome using the hkl planes with h, k, l all odd in crystals with the diamond structure, such as silicon and germanium; for this structure the structure factors [equation (2.3.7)] for the $2h,2k,2l$ reflections are zero so that there is no contamination by $\lambda/2$, and at the shorter wavelengths, $\lambda/3$ and so on, there are very few neutrons in the thermal neutron spectrum (Fig. 2.3.5).

Since 'perfect' crystals (of silicon and germanium, for example) have low reflectivity, for monochromator applications imperfect or 'mosaic' crystals are usually preferred. A mosaic crystal can be pictured as comprising small blocks of crystal with slightly differing orientations, the distribution in angle of these blocks being characterized by a full-width at half-maximum angle, β, known as the 'mosaic spread'. In addition to improving the intensity markedly,[12] this 'mosaic spread' will also increase the range of wavelengths obtained. Crystals intended for use as monochromators are very often deliberately deformed to achieve the desired mosaic structure. Further gains in intensity are sought by using vertically focusing monochromators, since the vertical divergence can be increased without serious detriment to the diffraction patterns. Vertically focusing monochromators usually comprise a number of separate monochromator crystals either individually adjustable (Fig. 2.3.17) or in fixed mountings on a bendable plate.

It is not common to find polarized neutrons being used in neutron powder diffractometers. Nevertheless, we think it appropriate to mention here that one means to obtain a polarized neutron beam is to use an appropriate polarizing crystal monochromator.[13] The 111 reflection from the ferromagnetic Heusler alloy Cu_2MnAl is commonly used for this purpose; the nuclear and magnetic structure factors [equations (2.3.7) and (2.3.8)] are of similar magnitude and they add or subtract depending on whether the neutron spin is antiparallel or parallel to the magnetization of the alloy. The beam reflected from such a monochromator can be polarized to better than 99%.

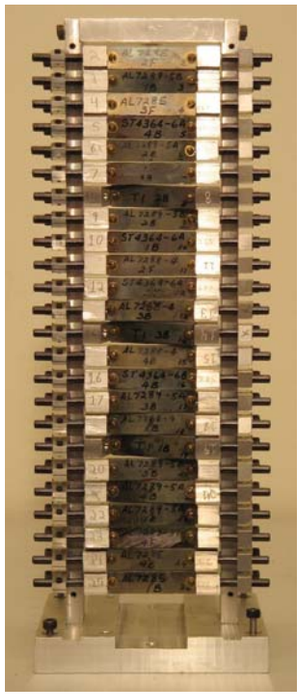

Figure 2.3.17
The vertically focusing monochromator constructed at the Brookhaven National Laboratory (Vogt *et al.*, 1994) and now used by the high-resolution powder diffractometer ECHIDNA at OPAL. The 24 monochromating elements are individually adjustable, and each of these is a 30-high stack of 0.3 mm thick Ge wafers, deformed to yield a suitable mosaic structure and then brazed together. (Reproduced with permission from ANSTO.)

The reader is referred to Section 4.4.2 of Volume C (Anderson & Schärpf, 2006) and to Kisi & Howard (2008) Sections 3.2.1 and 12.3 for further details.

2.3.4.1.3. *Neutron detectors*

Neutrons, being electrically neutral, do not themselves cause ionization and so cannot be detected directly; their detection and counting therefore depend on their capture by specific nuclei and the production of readily detectable ionizing radiation in the ensuing nuclear reaction. Only a limited number of neutron-capture reactions are useful for neutron detection [see Chapter 7.3 of Volume C (Convert & Chieux, 2006)]; they include

$$\begin{aligned}
{}^1_0\mathrm{n} + {}^3_2\mathrm{He} &\rightarrow {}^1_1\mathrm{H} + {}^3_1\mathrm{H} + 0.76\ \mathrm{MeV}\\
{}^1_0\mathrm{n} + {}^6_3\mathrm{Li} &\rightarrow {}^3_1\mathrm{H} + {}^4_2\mathrm{He} + 4.79\ \mathrm{MeV}\\
{}^1_0\mathrm{n} + {}^{10}_5\mathrm{B} &\rightarrow {}^7_3\mathrm{Li} + {}^4_2\mathrm{He} + 2.8\ \mathrm{MeV}\\
{}^1_0\mathrm{n} + {}^{157}_{64}\mathrm{Gd} &\rightarrow {}^{158}_{64}\mathrm{Gd} + \gamma\text{-rays} + \text{conversion electrons}\\
&\quad + \leq 0.18\ \mathrm{MeV}\\
{}^1_0\mathrm{n} + {}^{235}_{92}\mathrm{U} &\rightarrow \text{fission fragments} + \sim 200\,\mathrm{MeV}
\end{aligned}$$

(*cf.* Section 2.3.3.2).

[12] Most of the improvement is due to a change from a 'dynamical' to a 'kinematic' scattering regime.

[13] Polarized beams can also be produced using suitable mirrors or filters [see Section 4.4.2 of Volume C by Anderson & Schärpf (2006)].

The attenuation of neutrons in these materials (Section 2.3.2.4) will be dominated by the high absorption (by capture) cross sections (Table 2.3.2), so the linear attenuation coefficient will be given by $\mu = N\sigma_{\rm abs}$ where N is the number of absorbing nuclei per unit volume. We remark that absorption cross sections, with the exception of Gd, increase linearly with wavelength. The factor by which the neutron beam is diminished in a detector of thickness x is $\exp(-\mu x) = \exp(-N\sigma_{\rm abs}x)$. The detector efficiency, then, given by the fraction of neutrons absorbed (captured) in the detector, is $1 - \exp(-N\sigma_{\rm abs}x)$. In most cases the aim is to have high detector efficiency; however, in some circumstances it is desirable to monitor an incident neutron beam, in which case attenuation should be kept to a minimum. The account of neutron detection given here will be kept relatively brief since much has been written on this subject elsewhere [Oed, 2003; Chapter 7.3 of Volume C (Convert & Chieux, 2006)].

The task, following the neutron-capture reaction, is to detect the various charged particles or ionizing radiations that are produced. These are registered by the electrical signals they generate in a gas-filled proportional counter or ionization chamber, or in a semiconductor detector, recorded on film, or detected from the flashes of light they produce in a scintillator, for example ZnS. It is well worth noting that the secondary radiation carries no record of the energy of the detected neutrons; so whatever the means of detection, detectors can count neutrons but can provide no information on their energy distribution.

The gas-filled radiation detectors are essentially Geiger counters, comprising a gas-filled tube with a fine anode wire running along its centre. The anode collects the electrons released by ionization of the gas; if the anode voltage is high enough, there is a cascade of ionization providing amplification of the signal.[14] Detectors filled with boron trifluoride, $^{10}BF_3$, and helium-3, ^{3}He, have high efficiencies and are in common use; in these the nucleus designated to capture neutrons is incorporated in the filling gas. Such detectors operate with pulse-height discrimination, not in any attempt to determine neutron energy, but to discriminate against lower-voltage signals from γ-rays and other unwanted background. Another approach is to have a thin solid layer[15] of neutron-absorbing material, ^{235}U for example, releasing secondary radiation, in this case fission products, into a gas proportional counter filled with a standard argon/methane mixture; this would represent a low-efficiency neutron detector suitable for use as an incident-beam neutron monitor. Neutron detection based on semiconductor particle detectors is still in the developmental stage. The main problem is that the semiconductors used for charged-particle detection do not contain neutron-absorbing isotopes. Semiconductor particle detectors could be used to register the secondary radiation from an abutting layer of neutron-absorbing solid, but that layer would need to be thin, and another low-efficiency neutron detector would result. Scintillation detectors involve the placement of neutron-absorbing materials, such as ^{6}LiF, adjacent to a scintillator such as a ZnS screen, or perhaps the use of a Ce-doped lithium silicate glass, and counting the flashes of light that are produced. These light flashes can be recorded by photomultiplier tubes or on film. Scintillation detectors are, however, not used in constant-wavelength diffractometers because of their sensitivity to γ-radiation. They are used in time-of-flight diffractometers at spallation sources by exploiting the fact that the unwanted fast neutrons and γ-rays, and the thermal neutrons of interest, are separated in time (Section 2.3.4.2.2).

Much of the preceding description refers to single neutron counters, although it should be noted that there is a position-sensitive capability inherent in a film or scintillator screen. The earliest CW diffractometers employed just a single detector set on an arm that scanned through the scattering angle 2θ; the deployment of a Soller collimator just in front of the detector was advantageous. Conceptually the simplest but not necessarily the cheapest means for improvement was to mount a number of collimator/detector pairs on the detector arms. Such an improvement was made to diffractometer D1A at the Institut Laue–Langevin (Hewat & Bailey, 1976) by mounting ten sets of 10′ divergence Soller collimators/^{3}He detectors at intervals of 6°. The BT-1 diffractometer at NBSR operates with 32 ^{3}He detectors set at 5° intervals, so a scan through 5° covers a total angular range of 160°. The ultimate level for this kind of development was reached when D2B at the Institut Laue–Langevin operated in its former mode, with 64 detectors set at 2.5° intervals, each with its own 5′ Mylar Soller collimator; this required a scan through only 2.5° to record 160° of diffraction.

The alternative to using large numbers of individual detectors is to make use of position-sensitive neutron detectors (PSDs), and these have been in use for quite some time. The technology is that of the position-sensitive detection of charged particles, the important issue for neutrons being that the charged-particle detection should be located close to the neutron-capture event so that positional information is retained. A gas-filled ^{3}He detector with a single anode wire can serve as a linear PSD, for example by comparing the charges collected, after the capture event, at the opposite ends of the wire. The D2B diffractometer at the Institut Laue–Langevin has now been upgraded to 'SuperD2B', which uses 128 linear PSDs with their axes (anode wires) vertical, at 2θ intervals of 1.25°; this operates as a quasi-two-dimensional PSD. Diffractometers SPODI at FRM-II (80 detectors) and ECHIDNA at OPAL (128 detectors) are fitted with similar detector arrays. A single gas-filled chamber containing a number of separate parallel vertically aligned anodes, termed a multi-wire proportional counter (MWPC), provides another approach; the electronics needs to register at which of the wires the capture event occurred. This technology has extended from the first multi-wire PSD with 400 wires at 5 mm (0.2°) separation, used on the D1B diffractometer at the Institut Laue–Langevin in the 1970s, to a PSD with 1600 wires at 0.1° separation now in use on HRPT at SINQ (Fig. 2.3.15). A further advance is the development of the micro-strip gas chamber (MSGC) detector (Oed, 1988). In this detector the anodes and the cathodes are printed circuits on glass substrates, which are then mounted into the chamber. With this arrangement, an anode separation of 1 mm is achievable and the stability is excellent. The high-intensity diffractometer D20 at the Institut Laue–Langevin has a detector assembled from plates of micro-strip detectors and achieves 1600 anodes at 0.1° angle separation.

As pointed out above, the detection systems on SuperD2B, SPODI and ECHIDNA achieve a quasi-two-dimensional position capability by using banks of linear PSDs located side by side. An MWPC detector can achieve two-dimensional capability in a very similar manner, using the anode position to locate in the horizontal direction and charge division measurements at the ends of each anode wire to find the vertical position. An MWPC detector can also be fitted with segmented cathodes, either side of the anodes, one returning positional information in the horizontal

[14] Strictly speaking, the term 'Geiger counter' should be reserved for detectors operating in this amplification regime.
[15] The layer must be thin so that the secondary radiation, which has a short range in solids, can escape into the charged-particle detector.

direction and the other giving the vertical position. A detector of this kind is used on the WOMBAT diffractometer at the OPAL reactor. MSGC detectors can also be adapted to provide two-dimensional positional information after printing a set of cathodes orthogonal to the primary set on the back surface of the glass.

A few general comments about detecting systems are in order. The time for a detector to recover after registering a neutron count is known as the dead time, and this may be significant when count rates are high, in which case corrections are needed [Chapter 7.3 of Volume C (Convert & Chieux, 2006)]. For banks of detectors, and also for position-sensitive detectors, calibration for position and sensitivity becomes a critical issue. In the case of a smaller bank of detectors, it may be possible to scan the detector bank so the same diffraction pattern is recorded in the different detectors, in which case the relative positions and efficiencies of the different detectors can be determined quite well (see Section 4.1 of Kisi & Howard, 2008). For more extensive banks or large position-sensitive detectors, detector sensitivity calibration is performed by examining the very nearly isotropic incoherent scattering from vanadium. In this case checking for angular accuracy can be more difficult. The time taken to register a neutron count cannot be said to be a fundamental issue in CW powder diffraction, since in some applications it is scarcely relevant, although in other applications, such in the study of very fast reaction kinetics (Riley *et al.*, 2002), the constraints on time are very demanding.

2.3.4.1.4. *Resolution and intensity*

The resolution and intensity of a CW powder diffractometer are strongly influenced by the divergences α_1, α_2 and α_3 of the primary, monochromatic and diffracted beams, respectively, along with the mosaic spread β of the crystal monochromator. The situation was analysed by Caglioti *et al.* (1958) on the basis that the triangular transmission factor of each collimator, total width 2α, could be approximated by a Gaussian with full-width at half-maximum (FWHM) α, that the mosaic distribution of the monochromator could also be described by a Gaussian with FWHM β, but that there was no sample contribution to the peak widths. On this basis the diffraction peaks were found to be Gaussian, with the FWHM of the diffraction peak occurring at scattering angle 2θ given by (Hewat, 1975)

$$\mathrm{FWHM}^2 = U\tan^2\theta + V\tan\theta + W, \tag{2.3.18}$$

where

$$U = \frac{4(\alpha_1^2\alpha_2^2 + \alpha_1^2\beta^2 + \alpha_2^2\beta^2)}{\tan^2\theta_M(\alpha_1^2 + \alpha_2^2 + 4\beta^2)}, \tag{2.3.18a}$$

$$V = \frac{-4\alpha_2^2(\alpha_1^2 + 2\beta^2)}{\tan\theta_M(\alpha_1^2 + \alpha_2^2 + 4\beta^2)}, \tag{2.3.18b}$$

$$W = \frac{\alpha_1^2\alpha_2^2 + \alpha_1^2\alpha_3^2 + \alpha_2^2\alpha_3^2 + 4\beta^2(\alpha_2^2 + \alpha_3^2)}{\alpha_1^2 + \alpha_2^2 + 4\beta^2} \tag{2.3.18c}$$

and θ_M is the Bragg angle ($2\theta_M$ is the take-off angle) at the monochromator. Under these conditions the total (integrated) intensity in the diffraction peak is given by

$$L \propto \frac{\alpha_1\alpha_2\alpha_3\beta}{(\alpha_1^2 + \alpha_2^2 + 4\beta^2)^{1/2}}. \tag{2.3.19}$$

These equations have important implications and accordingly have received a good deal of attention. They return at once the well known resolution advantage in setting up the diffractometer in the parallel configuration (that seen in Fig. 2.3.15, in this configuration θ_M taken to be positive). Caglioti *et al.* (1958) deduced that for the simple case of $\alpha_1 = \alpha_2 = \alpha_3 = \beta = \alpha$ equations (2.3.18) and (2.3.19) reduce to

$$\mathrm{FWHM} = \alpha\left(\frac{11 - 12a + 12a^2}{6}\right)^{1/2} \text{ and } L \propto \alpha^3/(6)^{1/2},$$

where $a = \tan\theta/\tan\theta_M$; they went on to record results for a number of other combinations. In his design for a high-resolution diffractometer, Hewat (1975) considered the case $\alpha_2 = 2\beta > \alpha_1 \simeq \alpha_3$. Under these conditions, the peak widths are close to their minimum around the parallel focusing condition $\theta = \theta_M$, their widths there are given by

$$\mathrm{FWHM}^2 = \left(\alpha_1^2 + \alpha_3^2\right) - \frac{\alpha_1^4}{\alpha_1^2 + \alpha_2^2 + 4\beta^2} \simeq \alpha_1^2 + \alpha_3^2,$$

and the total intensity is approximately

$$L \propto \alpha_1\alpha_3\beta/(2)^{1/2}.$$

Hewat's conclusions, put briefly, were that good resolution could be obtained by keeping divergences α_1 and α_3 small, while intensity could be somewhat recovered by adopting relatively large values for the monochromator mosaic spread β and divergence α_2 of the monochromatic beam. Hewat also argued for a high monochromator take-off angle $2\theta_M$, not only to reduce peak widths [through the term $\cot\theta_M$ appearing in equation (2.3.17) and reappearing in equations (2.3.18)], but also to match the region of best resolution to that of the most closely spaced peaks in the diffraction pattern. Hewat's design was implemented in the D1A diffractometer at the Institut Laue–Langevin (Hewat & Bailey, 1976), subsequently in the D2B diffractometer at the same establishment, and elsewhere. In a version installed at the (now retired) HIFAR reactor in Sydney, Howard *et al.* (1983), using an Al_2O_3 (corundum) ceramic sample, reported a peak-width variation in close agreement with that calculated from equation (2.3.18). Although more sophisticated analyses are available in the literature (Cussen, 2000), this result would suggest that equations (2.3.18) still provide a good starting point.

The usual trade-off between intensity and resolution applies, and since neutron sources are rather less intense than X-ray sources, this is an important consideration. Intensity is sacrificed by using high monochromator take-off angles to limit the wavelength spread [equation (2.3.17)], and by using tight collimation [equation (2.3.19)]. Evidently intensities could be increased by relaxing these constraints. These days it is more common to build diffractometers of good-to-high resolution, and then to seek other means to improve data-collection rates. Focusing monochromators, such as described in Section 2.3.4.1.2, serve to increase the neutron intensity at the sample position without seriously degrading the resolution. In addition, the use of multi-detector banks and the development and deployment of position-sensitive detectors, as described in Section 2.3.4.1.3, has been very much driven by the desire to increase the speed of data collection. As mentioned earlier, the design and analysis of neutron powder diffractometers should be treated in a holistic fashion, and although some advanced analytical methods have been applied (Cussen, 2016 and references therein), Monte Carlo analyses using programs such as *McStas* (Willendrup *et al.*, 2014) and *VITESS* (Zendler *et al.*, 2014) to track large numbers of neutrons from the source right through to the neutron detectors are now widely employed.

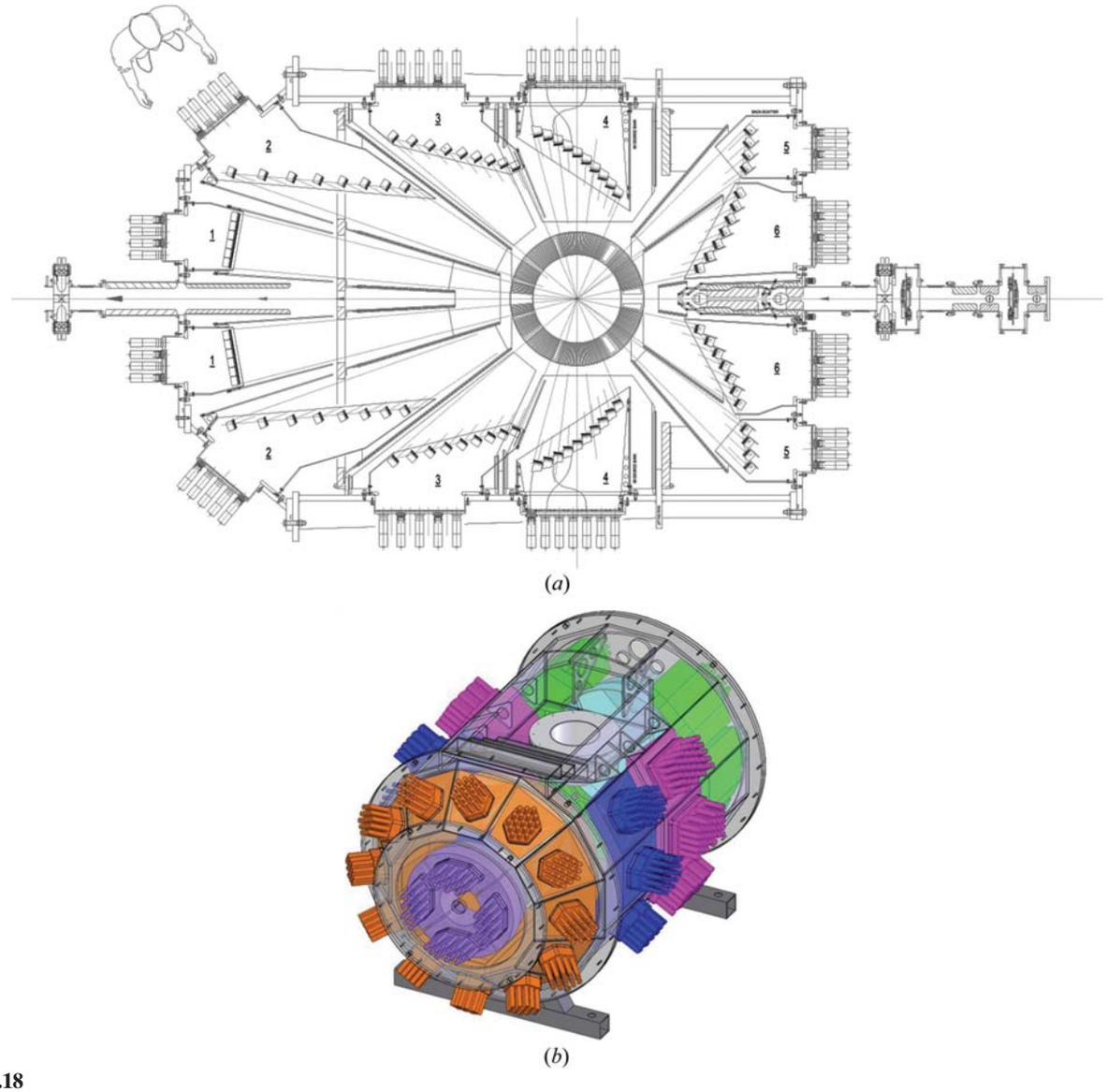

Figure 2.3.18
(*a*) Schematic cross section of the POLARIS diffractometer at the ISIS facility, UK, and (*b*) a three-dimensional solid model of the detector chamber. (Credit: STFC.)

2.3.4.2. *Time-of-flight (TOF) diffractometers*

Time-of-flight (TOF) diffractometers differ substantially from CW diffractometers. Neutrons delivered to the instrument are already partially collimated and TOF instruments have no monochromator and consequently no moving parts. The full incident neutron spectrum is utilized and needs to be well characterized in order to extract meaningful intensities; in addition the wavelength dependence of detector efficiencies needs to be taken into account. In principle, measurements from an incoherently (therefore isotropic and wavelength-independent) scattering sample such as V or H_2O provide the required characterization.[16] In practice, however, incident spectra are usually recorded using a low-efficiency detector (beam monitor) in the incident beam. Data from V are still required to correct for the relative efficiency of individual detectors or detector elements and their wavelength dependence (Soper *et al.*, 2000).

The basic components of a TOF powder diffractometer are the flight tube from the neutron source or a neutron guide, a precisely located sample position, banks of detectors at various positions around the sample position and a neutron-absorbing beam stop. In early TOF diffractometers, detector banks were relatively localized typically in forward scattering, close to $2\theta = 90^\circ$ and backscattering locations. More modern diffractometers have very extensive detector arrays such as the newly upgraded POLARIS instrument at the ISIS facility, which is illustrated in Fig. 2.3.18. Neutrons enter the diffractometer at the right of Fig. 2.3.18(*a*) through a number of adjustable neutron-absorbing jaws which trim the beam size to match the sample size. The beam is then incident on the sample, which is located within the chamber where the detectors, arranged in numbered banks, are housed. The entire sample/detector chamber (and flight tube) is evacuated during data collection in order to reduce absorption and scattering of the incident neutron beam by air, effects which both decrease the intensity of the neutrons incident on the sample and increase the background scattering. A human figure in Fig. 2.3.18(*a*) indicates the large scale of the device and it should be

[16] The much larger incoherent scattering cross section of H allows normalization data to be recorded much more quickly using H_2O; however, the small amount of additional moderation of the beam that occurs is usually considered undesirable.

noted that the substantial neutron shielding surrounding the detector chamber (known as the blockhouse) is not shown.

2.3.4.2.1. *Instrument resolution and design*

In a TOF instrument, all of the incident spectrum of neutron wavelengths is utilized, appropriately trimmed by the chopper system as previously described. The different wavelengths (λ) are identified through their time-of-flight (t) according to equation (2.3.15). Substituting that equation into Bragg's law, we obtain

$$d_{hkl} = \frac{ht}{2mL\sin\theta} = \frac{t}{505.554L\sin\theta} \quad (2.3.20)$$

for t in microseconds, d in ångstroms and L in metres.

The resolution of a TOF diffractometer is defined by the uncertainty in the d-spacing (Δd) relative to its absolute value d. Apparent as the width of the diffraction peaks, the resolution is given primarily by (Buras & Holas, 1968; Worlton *et al.*, 1976)

$$\frac{\Delta d}{d} = \left[\Delta\theta^2\cot^2\theta + \left(\frac{\Delta t}{t}\right)^2 + \left(\frac{\Delta L}{L}\right)^2\right]^{1/2}. \quad (2.3.21)$$

There are a number of important things to note concerning this equation:

(i) The terms $\Delta\theta\cot\theta$ and $\Delta L/L$ are fixed and independent of flight time once the diffractometer is constructed; in addition, as we have already noted (Section 2.3.3.3), for a spallation source with a suitably poisoned moderator the time resolution $\Delta t/t$ is practically constant. Thus the resolution of a TOF diffraction pattern is virtually constant across the entire range of d-spacing explored in a given detector bank.[17]

(ii) Uncertainties in the neutron path length, ΔL, can arise due to measurement uncertainty in determining L; however, these are usually overshadowed by the uncertainty that arises because neutrons can emerge into the neutron guide from any position within the finite-sized moderator and this uncertainty constitutes the major contribution to ΔL.

(iii) As ΔL is a constant, a linear improvement in resolution can be achieved merely by making the instrument longer, such as HRPD at ISIS and S-HRPD at J-PARC, which are almost 100 m long.

(iv) The contribution of the diffraction angle 2θ to resolution is considerable. For a fixed angular uncertainty (detector positioning and finite width) the $\cot\theta$ term varies from infinite at $2\theta = 0$ to zero at $2\theta = 180^\circ$. Therefore, the higher the detector angle, the better the resolution.

With these matters considered, we can return to our example of a modern TOF diffractometer in Fig. 2.3.18 and in particular the arrangement of the detectors. The strategy employed is to group multiple individual detector elements into a number of discrete banks. It may be seen from equation (2.3.21) that decreasing 2θ and increasing L have opposing effects on resolution. By appropriate manipulation of the equation and by expressing the overall neutron flight path as $L = L_1 + L_2$ where L_1 is the moderator-to-sample distance and L_2 is that from the sample to the detector, it is straightforward to obtain

$$L_2 = \Delta L\left[\left(\frac{\Delta d}{d}\right)^2 - \left(\frac{\Delta\theta}{\tan\theta}\right)^2 - \left(\frac{\Delta t}{t}\right)^2\right]^{-1/2} - L_1. \quad (2.3.22)$$

Therefore by adjusting 2θ and L_2 correctly, it is possible to construct banks of detectors covering a range of 2θ, for which the resolution is identical. This allows neutrons recorded in the entire detector bank to be 'focused' into a single diffraction pattern. The resulting curved detector arrangement is obvious in the high-resolution detector bank labelled 5 and 6 in Fig. 2.3.18(*a*). For a fixed (small) value of $\Delta d/d$, eventually space limitations impose restrictions on L_2 and a new, lower-resolution detector bank (4) commences. As the benefits of a curved arrangement become insignificant, the appropriate curve is approximated by a straight arrangement in the lower-angle banks and dispensed with altogether in the very low angle bank. In Fig. 2.3.18 the back-scattering (5, 6), 90° (4), two separate low-angle (2 & 3) and the very low angle (1) detector banks of POLARIS are identified. These have average 2θ angles of 146.72, 92.59, 52.21, 25.99 and 10.40°, respectively.

Raw diffraction patterns recorded in the various detector banks are compared in Fig. 2.3.19. Note that the curved background due to the incident spectrum is flattened when the patterns are normalized. A logarithmic scale is necessary to display the very wide range of d-spacings accessible across the whole instrument and this scale emphasises the near-constant resolution across each pattern. In keeping with equations (2.3.21) and (2.3.20), the effects of changing the detector angle are obviously greater resolution and access to shorter d-spacings as 2θ increases. Each detector bank can provide data for a different purpose according to its resolution and d-spacing coverage. For example, the combination of good resolution (4×10^{-3}) and a wide range of d-spacing (0.2–2.7 Å) makes data from the back-scattering bank (Fig. 2.3.19*e*) ideal for the refinement of medium- to large-scale crystal structures. The 90° bank (Fig. 2.3.19*d*) is optimized for use with complex sample environments such as high-pressure cells or reaction vessels, as this geometry combined with appropriate collimation of the incident and scattered neutron beams enables diffraction patterns to be collected that only contain Bragg reflections from the sample being studied. It can be used to obtain good-resolution data (7×10^{-3}) during a variety of *in situ* studies. The low-angle and very low angle banks with their access to very large d-spacings up to 20 Å are invaluable in determining unknown crystal structures and complex magnetic structures by allowing the indexing of low-index reflections and determining reflection conditions.

In order to reduce unwanted background counts and give better localization of the diffraction pattern from the sample, *i.e.* to better exclude sample environments such as cryostats or furnaces, the instrument is fitted with a radial collimator surrounding the sample position.[18] For more common sample environments, *e.g.* furnaces, this collimation allows all detector banks to view the sample unimpeded. The detector banks are contained within the large vacuum vessel shown in Fig. 2.3.18(*b*). This reduces attenuation and background due to scattering by air. The detector coverage on such an instrument is very large, in the case of POLARIS up to 45% of the available solid angle is covered. A full description of this instrument may be found in Smith *et al.* (2018).

[17] A small effect due to a time-dependent component of $\Delta t/t$ might be observed depending on the source and instrument configuration.

[18] Although typically constructed from planar vanes which are oscillated to average their shadow across all the detectors, the POLARIS collimator vanes are stationary, and are conical to follow the Debye–Scherrer cones of the diffracted neutrons.

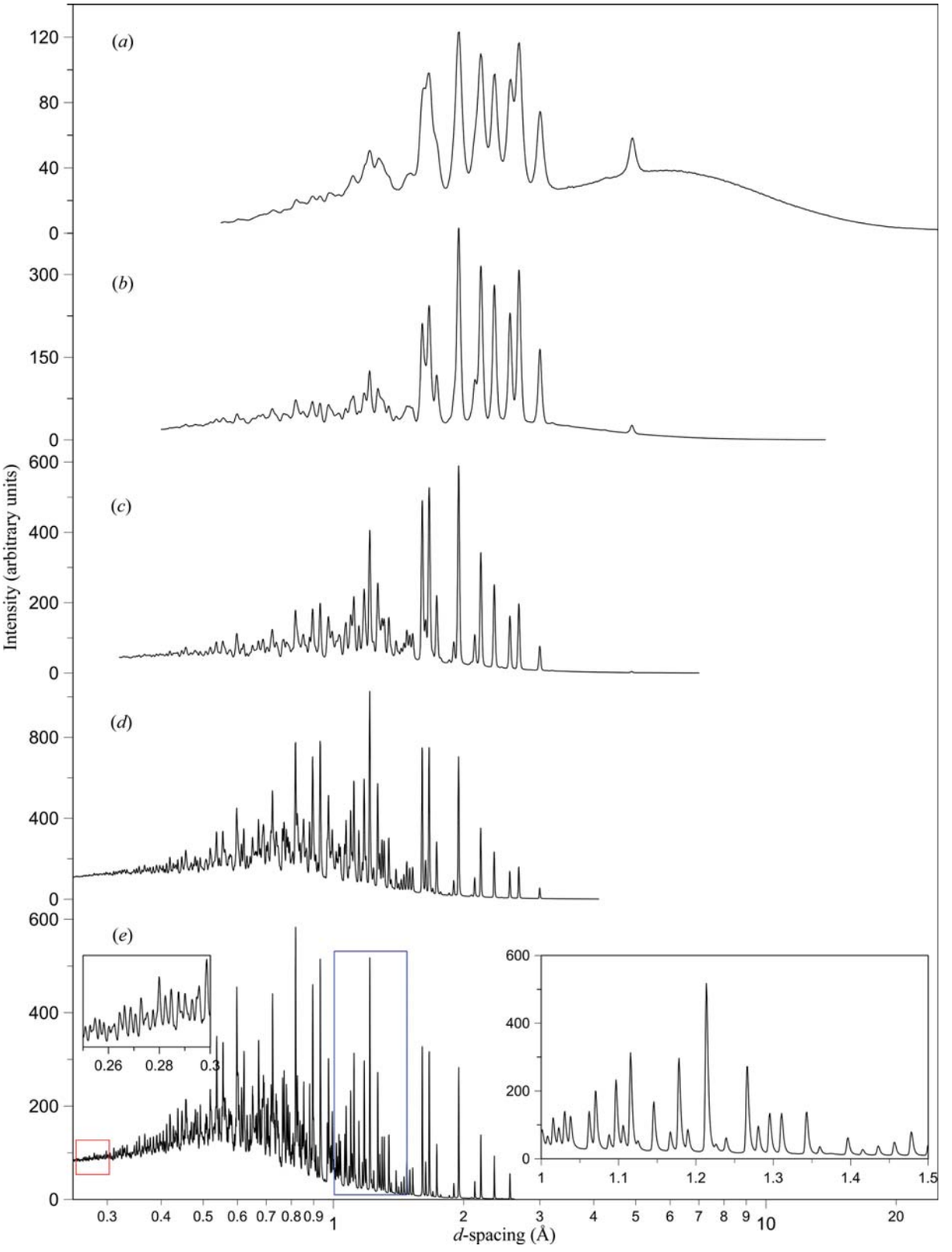

Figure 2.3.19
Raw neutron diffraction patterns from $Y_3Al_5O_{12}$ (YAG). Patterns from the five POLARIS detector banks, (*a*) very low angle, (*b*) low angle 1, (*c*) low angle 2, (*d*) 90° and (*e*) backscattering, are shown separately. Note that the very wide range of *d*-spacings accessible (~0.2–25 Å) necessitates the use of a $\log_{10}$ scale. Insets for the backscattering bank illustrate that useful data are obtained even at very small *d*-spacing (red) and that the resolution is very good (blue). Note the asymmetric peak shape that results from a rapid rise, followed by a slower exponential decay, in the number of neutrons emerging from the moderator after each incident proton pulse.

2.3.4.2.2. *Detection*

All the neutron detector types discussed in Section 2.3.4.1.3 are capable of detecting the scattered neutrons in a TOF pattern. Gas-filled proportional counters such as BF_3 and ^{3}He detectors have efficiencies governed by the neutron energy (or wavelength). Detectors on CW diffractometers are optimized for the narrow band of wavelengths available when using a crystal monochromator, say 1–2.4 Å. The wavelength range in TOF diffraction is generally much wider; as much as 0.2–6 Å or more,

and proportional detectors need to be specifically optimized. There is of course the added complexity of tracking the arrival time of each neutron and this has worked against the use of multi-wire proportional detectors and microstrip detectors as described in Section 2.3.4.1.3. Instead, there is extensive use of scintillation detectors, which are usually based on the ^{6}Li(n;t,α) reaction (Section 2.3.4.1.3). When doped into the ZnS film of a scintillator, the ^{6}Li provides excellent detection sensitivity and energy range. Discrimination against fast neutrons and γ-ray contamination in the incident beam is easily accommodated as these have different velocities to the thermal and epithermal neutrons used for TOF diffraction and are therefore readily excluded by the chopper system and detector electronics.

The detector electronics on older instruments recorded the diffraction pattern in a fixed set of time channels or bins; typically 1024 to begin with and progressively more as electronic and computational advances occurred. More recently, the technique has shifted to recording the data to memory in a continuous stream known as event mode, where the arrival time of each neutron is recorded. The user may then bin (and re-bin) the data into time channels to suit the resolution of the diffraction pattern, which may differ significantly from the instrument resolution because of microstructural features of the sample. Such features are discussed at length in Chapters 5.1 and 5.2.

In a new development, a neutron-sensitive microchannel plate detector has been developed (Tremsin, McPhate, Vallerga, Siegmund, Feller *et al.*, 2011). Microchannel plate detectors (MCPs) are divided into discrete pixels and record the arrival time of each neutron in each pixel. Initially used for high-resolution radiography at pulsed neutron sources, it was quickly realized that MCP detectors can be used for diffraction *via* the Bragg-edge phenomenon (Tremsin, McPhate, Vallerga, Siegmund, Kockelmann *et al.*, 2011). The resolution is typically 55 μm due to the data-acquisition electronics but can be sharpened to less than 15 μm using centroiding techniques. This type of detector opens the door to spatially resolved neutron powder diffraction in materials as well as strain-imaging applications on TOF neutron diffractometers.

2.3.4.3. *Variations on a theme*

The diffractometers HRPT (Fig. 2.3.15) and POLARIS (Fig. 2.3.18) are general-purpose instruments suitable for solving and studying medium-sized crystal structures under a range of non-ambient conditions and in some cases the study of non-crystalline or poorly crystalline materials. There are several such diffractometers at reactors [HB-2A at Oak Ridge (https://neutrons.ornl.gov/powder), D1B at ILL (https://www.ill.eu/instruments-support/instruments-groups/instruments/d1b/description/instrument-layout/), HRPD at KAERI (http://www.kaeri.re.kr:8080/english/sub/sub03_04_01_01.jsp), C2 at CINS (http://cins.ca/get-beam-time/beamline-specs/c2/)] and spallation sources around the world [POWGEN and NOMAD at SNS (https://neutrons.ornl.gov/powgen; https://neutrons.ornl.gov/nomad), GEM at ISIS (http://www.isis.stfc.ac.uk/instruments/gem/gem2467.html), iMATERIA at J-PARC (https://j-parc.jp/researcher/MatLife/en/instrumentation/images/BL20.gif) *etc*].

A more specialized type of TOF powder diffractometer is the High Resolution Powder Diffractometer (HRPD) at ISIS (https://www.isis.stfc.ac.uk/Pages/Hrpd.aspx) and a similar instrument, Super-HRPD at J-PARC (https://j-parc.jp/researcher/MatLife/en/instrumentation/images/BL08.jpg). Although both of these instruments have 90° and low-angle detector banks, their overall design has strongly centred on extremes of resolution, attaining $\Delta d/d$ values of 4×10^{-4} and 3×10^{-4}, respectively. Such extremes of resolution are attained primarily through making the flight path of both instruments nearly 100 m long and placing detectors at very high Bragg angles (150–176°). Data from these can supply individual peak positions to a precision of approximately 5 parts per million and whole pattern fitting can give correspondingly precise lattice parameters. Recalling that in TOF powder diffraction the resolution is constant across the whole pattern, this makes the instruments ideal for the solution of large crystal structures in which a great many diffraction peaks need to be resolved, for tracking phase transitions, and for solving structures involving pseudo-symmetry, which even in relatively small structures (*e.g.* perovskites) can be a challenge for lower-resolution instruments. Example diffraction patterns are shown in Fig. 2.3.20 for the structural transitions in $SrZrO_3$ (Howard *et al.*, 2000).

At the other extreme of instrument design are the very high intensity diffractometers exemplified by the CW instruments D20 at ILL (https://www.ill.eu/instruments-support/instruments-groups/instruments/d20/) and WOMBAT at ANSTO (http://www.ansto.gov.au/ResearchHub/Bragg/Facilities/Instruments/Wombat/). These diffractometers use a large degree of vertical focusing to greatly increase the incident flux on the sample and are fitted with large position-sensitive detectors from which the data can be stored at 1 MHz or faster. If there is a periodic time structure to the phenomenon under study due to some driving stimulus (*e.g.* a periodic laser, electric or magnetic field pulse), then the data can be analysed stroboscopically by synchronizing with the driving stimulus, giving an effective time resolution in the MHz range. Even in the absence of a periodic stimulus, useful diffraction patterns on these diffractometers can in favourable circumstances be stored at rates of 2, 10 or with a large enough sample even 50 Hz (Fig. 2.3.21).

It should be noted that for TOF diffractometers, the time structure imposed by the pulsed neutron source and chopper system places absolute limitations on the most rapid diffraction pattern that can be recorded. This is typically ~0.1 s at sources such as ISIS, J-PARC or SNS. An additional time penalty is often paid due to the time taken to save such large amounts of data (typically between 10 and 30 s). There is therefore no TOF equivalent of the very rapid stroboscopic mode of operation.

Other forms of specialized neutron powder diffractometer have also been developed. Among these are the engineering or residual stress diffractometers, exemplified by the TOF diffractometers ENGIN-X at ISIS (https://www.isis.stfc.ac.uk/Pages/Engin-X.aspx), VULCAN at SNS (https://neutrons.ornl.gov/vulcan), TAKUMI at J-PARC (https://j-parc.jp/researcher/MatLife/en/instrumentation/ns.html) and the CW diffractometers SALSA at ILL (https://www.ill.eu/instruments-support/instruments-groups/instruments/salsa/description/instrument-layout) and KOWARI at ANSTO (http://www.ansto.gov.au/ResearchHub/Bragg/Facilities/Instruments/Kowari/). The purpose of these diffractometers is to measure accurate interplanar spacing (d) within a small gauge volume defined by the intersection of incident and diffracted beams inside a larger sample, as illustrated for constant wavelength in Fig. 2.3.22.

Variations in the d-spacing relative to a strain-free reference value (d_o) represent the average strain in the gauge volume parallel to the scattering vector (*i.e.* perpendicular to the diffracting planes) as is also illustrated in Fig. 2.3.22. By determining strains in several directions, it is possible to reconstruct the full strain tensor within each gauge volume, and

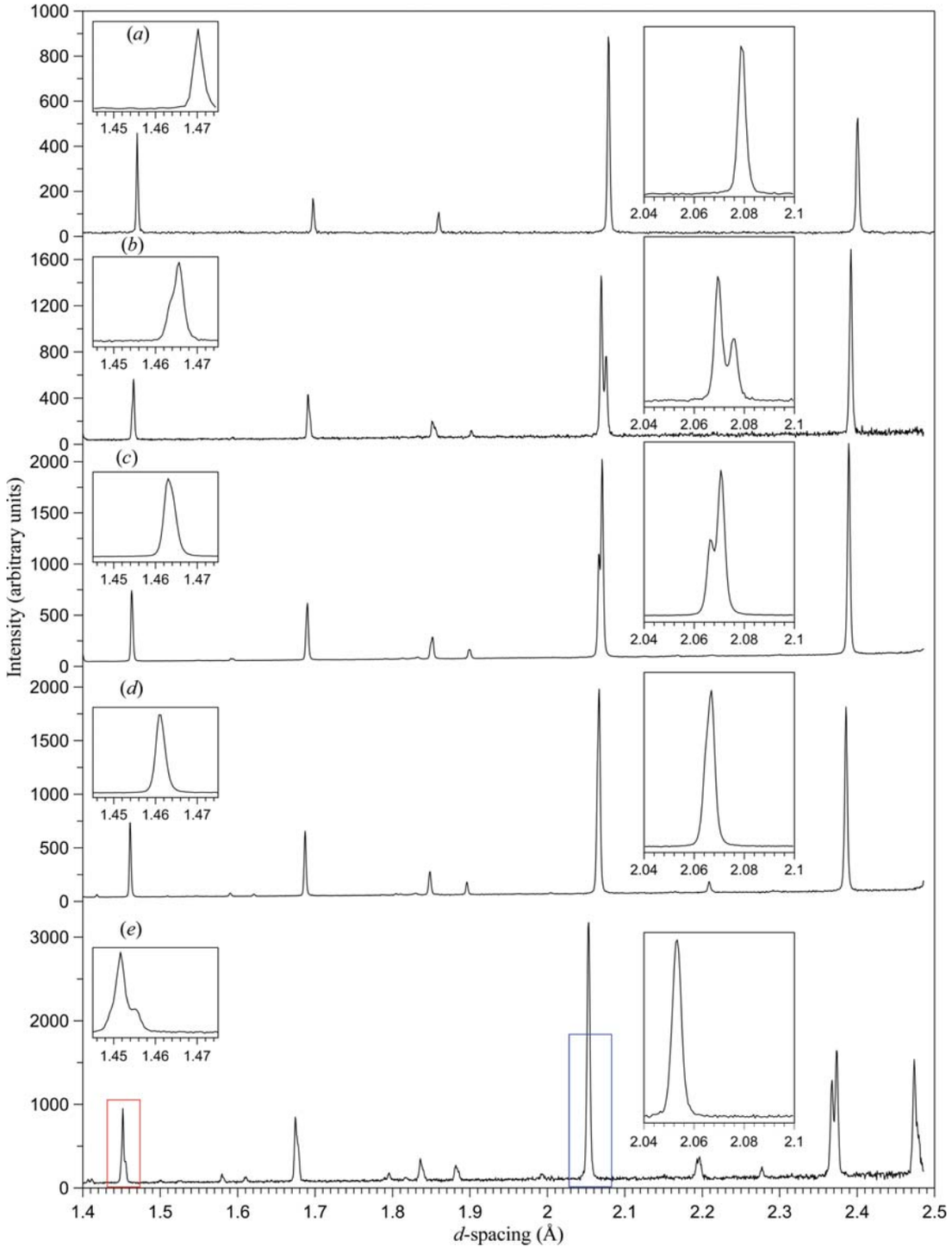

Figure 2.3.20
Parts of the very high resolution neutron powder-diffraction patterns recorded by the backscattering detector bank on the instrument HRPD at ISIS from $SrZrO_3$ at (*a*) 1403, (*b*) 1153, (*c*) 1053, (*d*) 933 and (*e*) 293 K. Insets to the left and right show subtle changes to the reflection shapes and splitting of reflections due to phase transitions from the cubic ($Pm\bar{3}m$) in pattern (*a*), to the tetragonal phase ($I4/mcm$) in (*b*), an orthorhombic phase (*Imma*) in (*c*) and a second orthorhombic phase (*Pnma*) in (*d*) and (*e*). Note the intensity reversal in the 002 reflection (right insets), which was pivotal in finding and solving the orthorhombic phase in *Imma* (Howard *et al.*, 2000).

this may be converted into the stress tensor, the desired outcome for engineering purposes (Noyan & Cohen, 1987; Fitzpatrick & Lodini, 2003; Kisi & Howard, 2008). This procedure is widely used in residual stress analysis to study stress distributions in fabricated or welded components and also to observe the internal stress distribution due to an externally imposed load. An example is illustrated in Fig. 2.3.23 in relation to *in situ* experiments and the stress distribution in granular materials.

The required localization of the gauge volume is achieved by shaping the incident and diffracted beams with slits/collimators and is greatly assisted by fixing the diffraction angle 2θ at $\pm 90^\circ$. In CW instruments, the need for high resolution and good intensity is met by using a focusing (bent Si) monochromator and a small area detector to record the data. This generally limits the investigation to a single Bragg peak (reflection), the position of which is carefully mapped over the sampled area for each strain component under investigation.

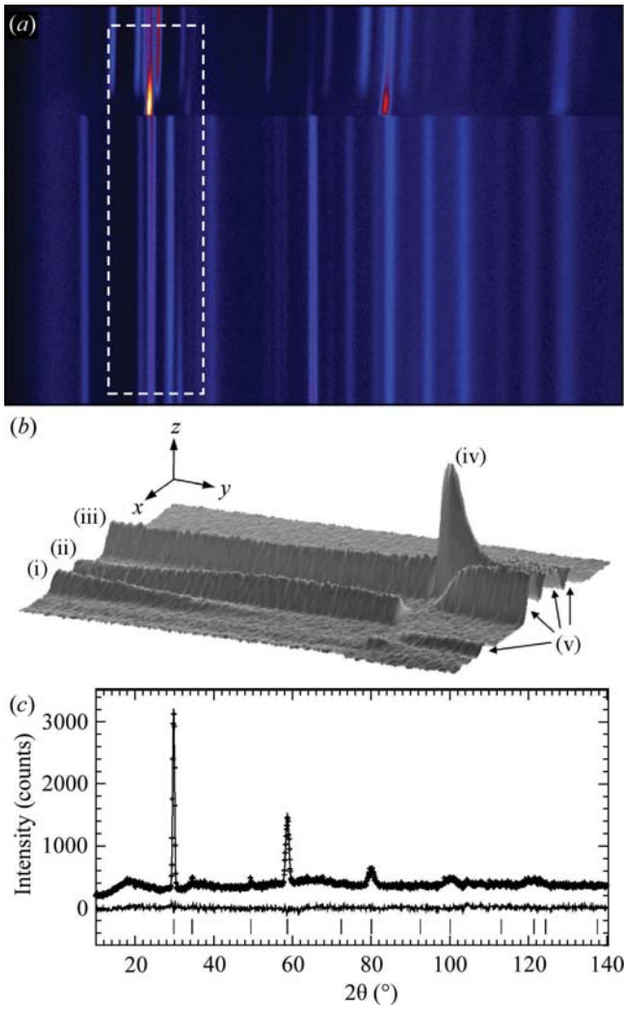

Figure 2.3.21
Neutron powder-diffraction patterns during combustion synthesis of Ti_3SiC_2 recorded in 400 ms each on the diffractometer D20 at ILL (Riley *et al.*, 2002). Panel (*a*) shows an overview of the reaction process with time vertical, diffraction angle horizontal and intensity as colour/brightness. Panel (*b*) is a three-dimensional view of the portion enclosed by dashed lines in (*a*), representing 140 s of reaction, wherein the numbered reflections show (i), (ii) a phase change in Ti, (iii) SiC, (iv) formation of an intermediate phase Ti(Si,C) and (v) growth of the Ti_3SiC_2 product. Panel (*c*) illustrates *via* Rietveld refinement the high quality of diffraction patterns even on this short timescale.

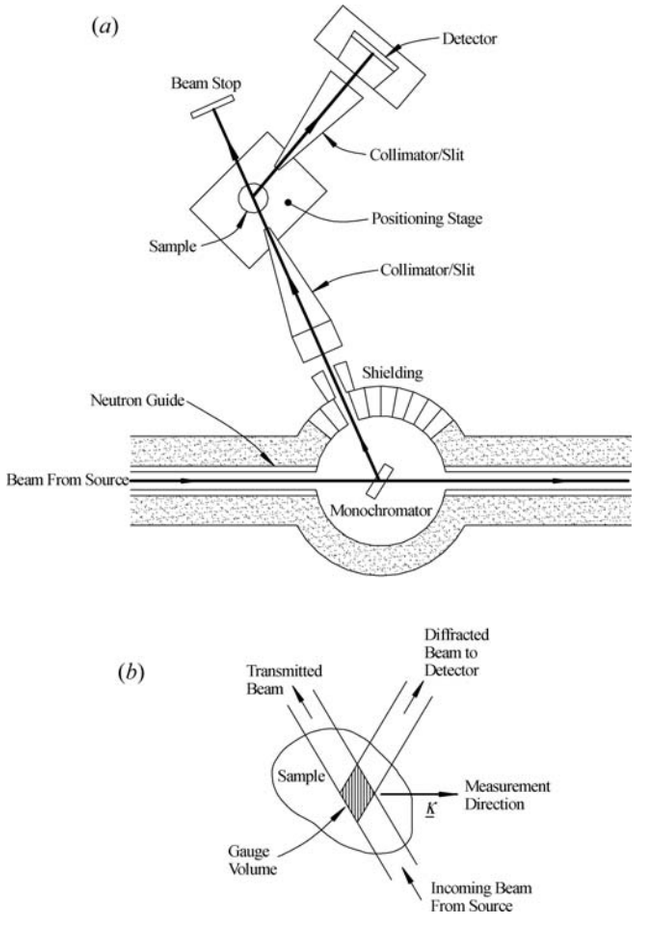

Figure 2.3.22
Illustrating (*a*) a CW engineering diffractometer and (*b*) the formation of a gauge volume at the intersection of the incident and diffracted beams.

TOF engineering diffractometers record a full diffraction pattern at each position. Localization of the gauge volume is achieved using symmetric detector banks and radial collimators on either side of the sample position (Fig. 2.3.24). All other instrument-design criteria are generally secondary to this, as a parallelepiped-shaped gauge volume allows a seamless strain (stress) map to be obtained. These instruments are usually 40–50 m long and have moderately high resolution, which allows peak positions and hence strains to be measured to a precision of 5×10^{-5} in favourable circumstances. In common engineering materials (steels, aluminium alloys *etc.*) this equates to an absolute minimum stress uncertainty of 4–10 MPa. The extreme resolution that would be available using very high resolution designs like HRPD and Super-HRPD (above) is sacrificed in order to obtain data on a reasonable timescale given the generally small gauge volume (0.5–30 mm^3) and the need to map the strain field piecewise over an extended region of the sample.

Although it is not usual for instruments to be specifically designed for the purpose, neutron diffraction is also particularly useful for studying crystallographic texture in materials, as the neutron-diffraction pattern is not distorted by surface coatings or preparation methods. In principle, any diffractometer can be used for measuring texture simply by recording a large number of diffraction patterns with the sample rastered in small angular intervals (5° is common) about two mutually perpendicular axes to form a grid over all orientations. This is extremely time consuming on a conventional CW diffractometer, although the whole pattern is captured each time, as the intensity recorded for the different reflections is subject to different corrections. This can be greatly sped up by using a CW engineering diffractometer (SALSA, KOWARI) with an intense, well collimated incident beam and fitted with an area detector. For example, on KOWARI, the detector spans 15° in both horizontal and vertical directions and so the sample needs to be re-positioned far fewer times. An added advantage is that the diffraction geometry is identical for each sample position and almost so for each reflection studied, and so a pure (*i.e.* model-independent) texture measurement is obtained. Texture measurements on modern TOF diffractometers (*e.g.* GEM, POLARIS, POWGEN, NOMAD and iMATERIA) are in principle quite straightforward. Because there are detectors in many positions all around the sample, the scattering vector and hence orientation of diffracting planes (crystal orientation) is sampled in many orientations all in one data collection. If data from the individual detectors are not 'focused' into composite diffraction patterns as for crystal-structure studies, then very few re-orientations are required to record data representing the full texture. However, since each reflection in each detector bank is sampled using

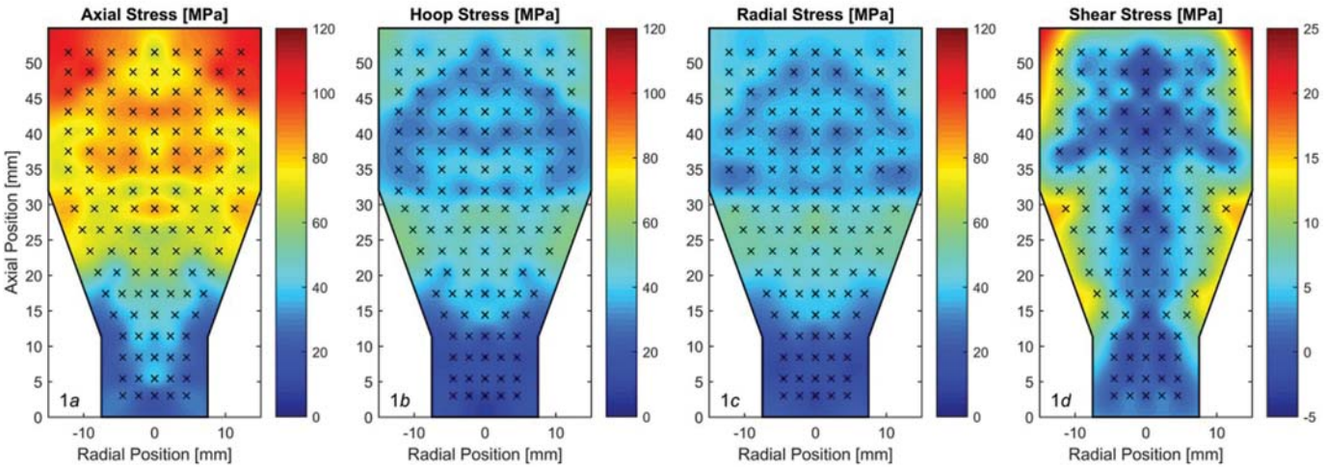

Figure 2.3.23
Stress distribution for four stress components in an iron powder compacted within a convergent die (see also Zhang *et al.*, 2016).

neutrons of different wavelength, each is recorded under different conditions for attenuation and extinction. In addition, to make full use of all the data, whole pattern or Rietveld analysis using a preferred-orientation (texture) model has to be conducted for each of the multitude of diffraction patterns recorded. As well as being time consuming, the reliability of the resultant pole figures and orientation density function is governed by the quality of all the individual models (for background, peak shape, peak width, sample centring, attenuation *etc*.) within the Rietveld refinement as well as the ability of the preferred-orientation model in the Rietveld program to accurately fit the real texture. A pure model-independent texture measurement can only be obtained using CW or TOF single-peak methods.

The instrument WISH at ISIS represents a departure from the normal TOF diffractometer design in that it receives *long wavelength* neutrons (1.5–15 Å) from a cold neutron source at Target Station 2. Ballistic supermirror neutron guides and three choppers deliver neutrons in an active bandwidth of 8 Å for a given chopper setting (https://www.isis.stfc.ac.uk/Pages/Wish.aspx). The pixelated ^{3}He detectors cover Bragg angles in the very wide range 10–170°. WISH is designed for the study of complex magnetic structures and large-unit-cell structures in chemistry and biology. Polarization analysis is available to assist the former.

The concept of long-wavelength neutron powder diffraction will be taken a step further in the DREAM instrument planned for the European Spallation Source (ESS, https://europeanspallationsource.se/realizing-dream-versatile-powder-diffractometer). This instrument will receive neutrons simultaneously from *thermal* and *cold* neutron moderators. It will have a complex array of choppers to shape the incident pulse prior to arrival at the sample. Modelling has indicated that intensity gains of a factor of 10–30 are to be expected and that the instrument may be able to deliver $\Delta d/d$ as low as 4×10^{-5}, albeit at very long wavelengths. More typically the projection is that $\Delta d/d$ as low as 1×10^{-4} could be achieved with more conventional wavelengths. Perhaps the major advantage of the instrument will not be its absolute resolution but the ability to change resolution over the full range during the experiment by simply altering the chopper settings. Therefore unexpected phenomena (phase transitions *etc*.) can be tracked during the initial experiment with no time lost by having to prepare a proposal for a different higher-resolution instrument.

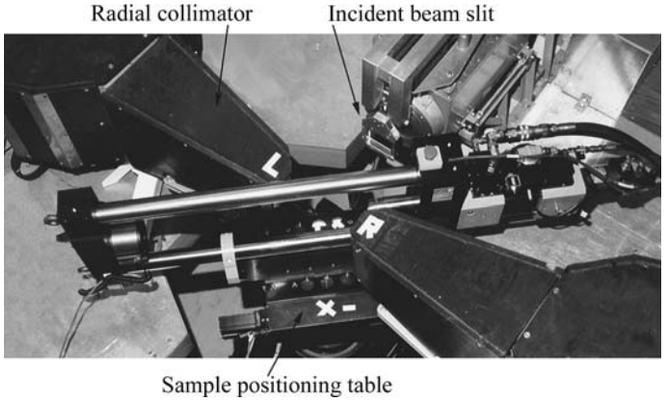

Figure 2.3.24
The engineering diffractometer ENGIN-X at ISIS. The incident beam enters through the flight tube at the top and the left (L) and right (R) 90° detector banks simultaneously record patterns with the scattering vector perpendicular and parallel to the sample axis, respectively. A mechanical testing machine used for *in situ* application of loads is also shown (https://www.isis.stfc.ac.uk). (Credit: STFC.)

2.3.4.4. *Comparison of CW and TOF diffractometers*

The preceding discussion has demonstrated that, although not necessarily the case for other types of neutron scattering, powder diffraction can be very successfully conducted on either CW or TOF instruments. Their relative advantages for the various types of powder-diffraction experiment are embedded in the discussion above and summarized in Table 2.3.5.

Plotting and summarizing the approximate intensity and resolution of different types of neutron diffractometer may be of assistance in assessing the options (Fig. 2.3.25). In the figure, resolution is shown as the inverse of the FWHM ($\Delta d/d$) and intensity is shown as the inverse of the time in seconds taken to record a single diffraction pattern, so that improvements follow the positive x and y axes.

There are two particular cases where the distinction between CW and TOF instruments can determine the success or failure of a neutron powder-diffraction experiment. The first is where crystal structures or phase transitions involving extreme pseudosymmetry are being studied. In this case, the very high resolution available over the entire Q-range (d-spacing range) using high-resolution TOF instruments such as HRPD at the ISIS

Table 2.3.5
Advantages of CW and TOF instruments (modified from Kisi & Howard, 2008)

CW	TOF
(1) Incident beam may be essentially monochromatic, in which case the spectrum is well characterized	(1) The whole incident spectrum is utilized, but it needs to be carefully characterized if intensity data are to be used
(2) Large d-spacings are easily accessible for study of complex magnetic and large-unit-cell structures	(2) Data are collected to very large Q values (small d-spacings)
	(3) Few cold neutron instruments are available for study of complex magnetic and large-unit-cell structures
(3) Can fine tune the resolution during an experiment	(4) Resolution is constant across the whole pattern
	(5) Very high resolution is readily attained by using long flight paths
(4) More common	(6) Complex sample environments are very readily used if 90° detector banks are available
(5) Peak shapes are simpler to model	
(6) Absorption and extinction corrections are relatively straightforward	(7) Simpler to intersect a large proportion of the Debye–Scherrer cones with large detector banks
(7) Data storage and reduction is simpler	
(8) Extremely rapid data collection and stroboscopic measurements are feasible	(8) Very fast data collection is feasible
(9) Engineering diffractometers are very well suited for strain scanning in complex objects	(9) Engineering diffractometers use an extended diffraction pattern, ideal for *in situ* loading and/or heating
(10) Texture is straightforward to measure on engineering diffractometers	(10) Texture can be measured on universal instruments

facility (UK) or SuperHRPD at J-PARC confers a particular advantage. The CW equivalent high-resolution powder diffractometers such as D2B at ILL and ECHIDNA at ANSTO can almost match the absolute resolution of the TOF instruments, D2B achieving $\Delta d/d$ of 5.6 $\times$ 10^{-4}; however, the resolution function for a CW diffractometer [equation (2.3.18)] has a strong minimum and so this resolution can only be achieved over a restricted range of d-spacing. The reflections appearing in the highest-resolution zone can be shifted by wavelength changes, which of necessity require re-recording of the pattern.

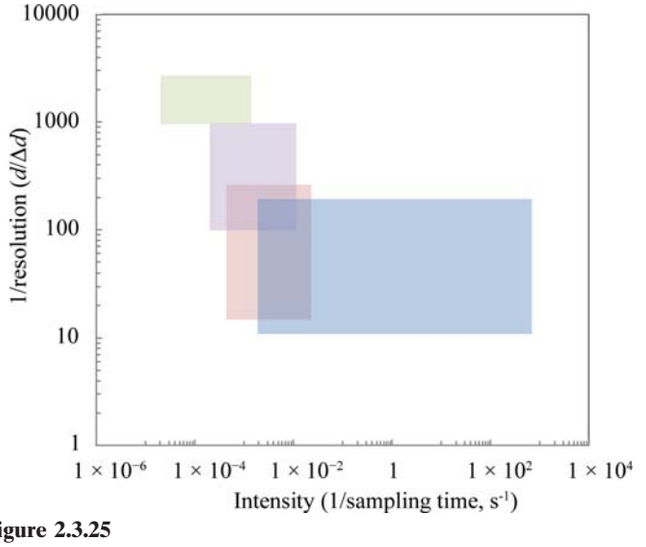

Figure 2.3.25
Schematic showing regions of intensity–resolution space in which different diffractometer types typically operate. High-resolution TOF diffractometers operate in the green area, engineering diffractometers (TOF or CW) in the purple area, multi-purpose TOF diffractometers such as POLARIS in the orange area and very high intensity CW diffractometers in the blue area.

The second extreme case is when rapid kinetic behaviours are to be studied. In this case, a small number of CW diffractometers (*e.g.* D20 at the Institut Laue–Langevin or WOMBAT at ANSTO) have a distinct advantage. Therefore at this time, processes that occur reproducibly and uniformly over a large sample on sub-1 s timescales are best suited to stroboscopic studies using one of the very rapid CW diffractometers available. There are nonetheless a great number of processes that can be studied on the timescales accessible using TOF, where near-constant resolution across the entire diffraction pattern lends considerable advantage.

If unaffected by extremes of resolution, intensity or highly specialized data types (stress, texture *etc.*), the choice between a CW or TOF instrument can be made based more casually on proximity to neutron sources and the access arrangements for national or regional neutron users.

2.3.5. Experimental considerations

2.3.5.1. *Preliminary considerations*

Neutron-diffraction studies are motivated by a desire to exploit the unique properties of neutrons as listed in Sections 2.3.1 and 2.3.2. As access to neutron diffraction is carefully regulated through an experiment proposal system, considerable planning is required in order to write a successful proposal. Owing to the expense of operating a neutron source and pressure on instrument time, there is an onus on the experimental team to make the best use of neutron beam time. Consideration should be given to the type of instrument required, the resolution that is needed, the d-spacing range of interest, how long each pattern will take to record, the requirement (or not) for standard samples and whether a special sample environment is needed.

references